ACS Sustainable Chemistry & Engineering

Research Article

pubs.acs.org/journal/ascecg

pH-Responsive Polyoxometalate-Based Supramolecular Hybrid Nanomaterials and Application as Renewable Catalyst for Dyes

Yanjun Gong,[†,⊥] Yongxian Guo,[†,⊥] Qiongzheng Hu,[‡] Chen Wang,[§] Ling Zang,[§] and Li Yu*[,†]

[†]Key Laboratory of Colloid and Interface Chemistry, Shandong University, Ministry of Education, No. 27 Shanda Nanlu, Jinan 250100, PR China

[‡]Department of Chemistry, University of Houston, Houston, Texas 77204, United States

[§]Nano Institute of Utah and Department of Materials Science and Engineering, University of Utah, Salt Lake City, Utah 84112, United States

Supporting Information

ABSTRACT: Keggin-type polyoxometalate (POM), phosphotungstic acid ($H_3PW_{12}O_{40}$), was encapsulated by an oppositely charged COOH-functionalized surface active ionic liquid (SAIL), *N*-decyl-*N*′-carboxymethyl imidazolium bromide ([*N*-C_{10}, *N*′-COOH-Im]Br), with the assistance of an ionic self-assembly (ISA) process in an aqueous environment. The as-prepared POM/SAIL material possesses multiple active properties, including reversible pH-response and renewable catalyst for dye degradation. Specifically, the POM-based hybrid materials show a great enhancement in catalytic efficiency when it is employed in degradation of methyl orange (MO) in aqueous solution. Furthermore, the electrostatic repulsions between POM and the deprotonated SAIL may result in the pH-induced disassembly and assembly of the hybrid nanomaterials, which provides an expedient method to regenerate the catalytic activity. Therefore, the presented POM/SAIL hybrid materials are expected to improve the common poisoning issue of the traditional heterogeneous catalysts for industrial applications.

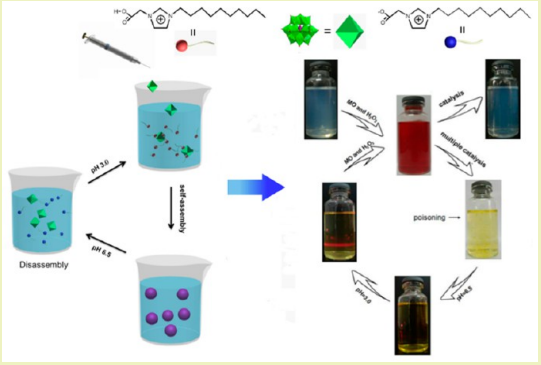

KEYWORDS: *Self-assembly, Polyoxometalate, Surface active ionic liquid, pH-Responsive, Renewable catalyst*

INTRODUCTION

The supramolecular self-assembly process offers a versatile route for the fabrication of well-defined and discrete materials at nanoscopic scales, and therefore facilitates the in-depth research of various new materials, such as nanomaterials, organogels, organic−inorganic hybrid materials, and biomolecular materials.[1−4] Among them, due to the combined properties from inorganic and organic components, the supramolecular self-assembled organic−inorganic hybrid materials have drawn particularly research interest.[5,6] Within such materials, the inorganic fraction can enhance mechanical strength and build additional functionalities (e.g., specifically catalytic, optical, and electric properties) into nanomaterials, while the organic fraction is capable of self-assembling and shows tendency of coassembling with inorganic fraction into nanomaterials.

Polyoxometalate (POM), an intensively studied class of anionic oxide nanoclusters of transition metals, are emerging as useful materials for potential applications in diverse field such as catalysis,[7,8] electronics,[9,10] optics,[11,12] medicine,[13] sensing[14,15] and biology,[16,17] etc. On the other hand, surface active ionic liquids (SAILs), referred to the ionic liquids (ILs) containing long alkyl chains that exhibit an amphiphilic characteristic, have emerged as a novel type of amphiphiles. Compared to traditional surfactants, SAILs usually display superior surface active properties and specific phase behaviors in the aqueous phase. Additionally, SAILs are a kind of green and environmentally friendly compounds. Therefore, SAILs are desirable building blocks for various well-defined supramolecular structures.[18]

POM and SAILs have been extensively applied as nanoscale building blocks for construction of hybrid inorganic−organic materials.[19−23] For example, Wang's group designed POM-based hybrids via partial replacement of the protons in POM with cations of ILs.[24] Biboum et al. reported a method to construct hybrid materials from poly(ionic liquid) and POM.[25] However, beyond the POM/SAIL structural design, attempts to design functionalized POM/SAIL structures, for example, a smart catalyst with stimuli-responsive ability and catalytic renewability, have been barely reported.

Herein, we report on a green and model synthesis method to prepare supramolecular nanomaterials based on an ionic self-assembly (ISA) strategy.[26] The supramolecular complex consists

Special Issue: Asia-Pacific Congress on Catalysis: Advances in Catalysis for Sustainable Development

Received: November 18, 2016
Revised: December 28, 2016
Published: January 6, 2017

DOI: 10.1021/acssuschemeng.6b02791
ACS Sustainable Chem. Eng. 2017, 5, 3650−3658

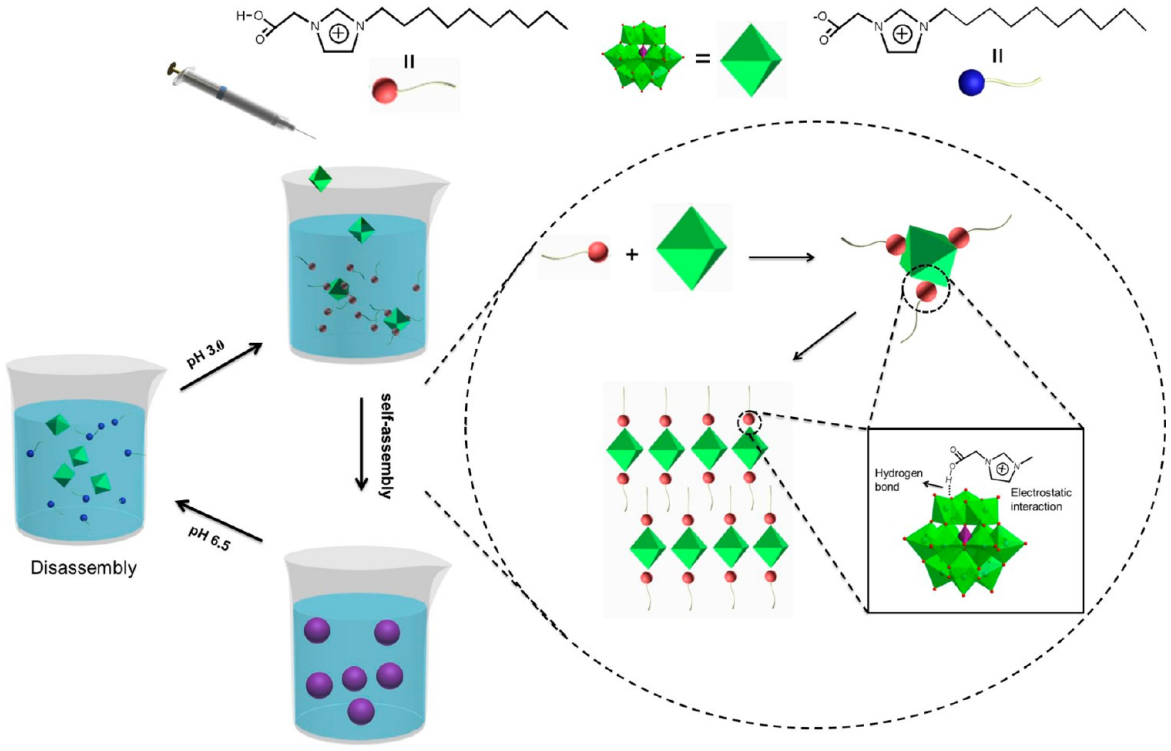

Figure 1. Schematic illustration of the formation mechanism of POM/[*N*-C_{10}, *N*′-COOH-Im]Br hybrid materials and the reversible disassembly and assembly processes induced by changing pH in the aqueous solution.

of a Keggin-type POM, phosphotungstic acid ($H_3PW_{12}O_{40}$), and COOH-functionalized imidazolium-based SAIL, *N*-decyl-*N*′-carboxymethyl imidazolium bromide ([*N*-C_{10}, *N*′-COOH-Im]Br). Figure 1 shows the proposed formation mechanism of the supramolecular material coassembled from [*N*-C_{10}, *N*′-COOH-Im]Br molecules and POM clusters in water. Initially, POM and [*N*-C_{10}, *N*′-COOH-Im]Br form IL-encapsulated POM supramolecular complexes through electrostatic interactions and H-bond. Subsequently, these supramolecular complexes can self-assemble into hybrid materials due to hydrophobic interactions between long hydrocarbon chains of ILs decorated on the POM clusters. Therefore, the as-prepared materials could inherit electrochemical properties from POM parts, as well as exhibit pH-responsive properties, that the pH can induce disassembly and assembly of the hybrid nanospheres due to electrostatic repulsions between POM and the deprotonated IL molecules.

Numerous chemical reactions can be catalyzed by POM due to their controllable redox potentials and electron transfer, and this feature is also well kept in POM-based materials.[27−30] Heterogeneous catalysis is widely used for industrial purposes because it is easy to operate and the catalyst can be easily separated and recycled. However, poisoning of heterogeneous catalyst is almost universal and causes huge losses in industry. Here, based on the pH-responsive property, the poisoning issue of hybrid materials can be addressed by controlling their disassembly and assembly processes in the aqueous solution with different pH, so that the formed solid-state catalyst can be efficiently recycled. In the process of ISA, both electrostatic interactions and hydrogen bonds play important roles in the formation of POM/[*N*-C_{10}, *N*′-COOH-Im]Br materials. These interactions can also improve the electron transfer rate from organic substrates to POM. Herein, we demonstrated catalytic activity of the hybrid materials in the aqueous solution by using the catalytic degradation of methyl orange (MO) in dark, and H_2O_2 was used as an ecofriendly oxidant in the catalytic reaction.

EXPERIMENTAL SECTION

Materials. Phosphotungstic acid (99%) was purchased from J&K Chemical Technology, China. 1-Bromodecane (98%), 1-bromododecane (98%), 1-bromotetradecane (98%), 1-bromohexadecane (99%), *N*-alkylimidazole (99%), and bromoacetic acid (99%) were all bought from Aladdin Chemistry Co., Ltd., of China. Benzophenone (chemical pure) was obtained from Sinopharm Chemical Reagent Co., Ltd., of China. All the above reagents were used without further purification. Triply distilled and deionized water was used in all the experiments.

Synthesis of COOH-Functionalized Imidazolium SAILs. *N*-Alkyl-*N*′-carboxymethyl imidazolium bromides ([*N*-C_n, *N*′-COOH-Im]Br, n = 10, 12, 14, 16) were prepared as improved procedures according to our early report.[18] *N*-Alkylimidazole was prepared based on the previous description.[18] Take [*N*-C_{12}, *N*′-COOH-Im]Br as an example. ^{1}H NMR (D_2O, ppm): δ = 8.80 (s, 1 H, CH), 7.46 (d, 1 H, CH), 7.46 (d, 1 H, CH), 4.88 (s, 2 H, CH_2), 4.18 (t, 2 H, CH_2), 1.83 (m, 2 H, CH_2), 1.27 (m, 18 H, CH_2), 0.80 (t, 3 H, CH_3). Calcd for [*N*-C_{12}, *N*′-COOH-Im]Br: C, 69.40; H, 10.20; O, 10.88; N, 9.52. Found: C, 69.25; H, 10.78; O, 10.72; N, 9.25.

Preparation of Supramolecular Structures. Aqueous solutions of POM (10 mL, 0.5 mM) and [*N*-C_{10}, *N*′-COOH-Im]Br (30 mL, 0.5 mM) were mixed and stirred in a 50 mL flask. After additional stirring for different time, the mixture was placed in a thermostatic water bath with the uncertainty of within ±0.1 °C. The obtained products were collected by filtration, washed three times with water to remove salts and possible precursors. The final products were dried under vacuum at 55 °C for 24 h.

Electrochemical Measurements. Cycle voltammetry (CV) was used to detect the electrochemical properties of the supramolecular material. Diluted sulfuric acid solution (pH = 1) and a standard three-electrode cell (Ag/AgCl electrode as the reference electrode, a platinum plate as the counter electrode, the glassy carbon disc as the working electrode) were used during the processes of determination.

DOI: 10.1021/acssuschemeng.6b02791
ACS Sustainable Chem. Eng. 2017, 5, 3650−3658

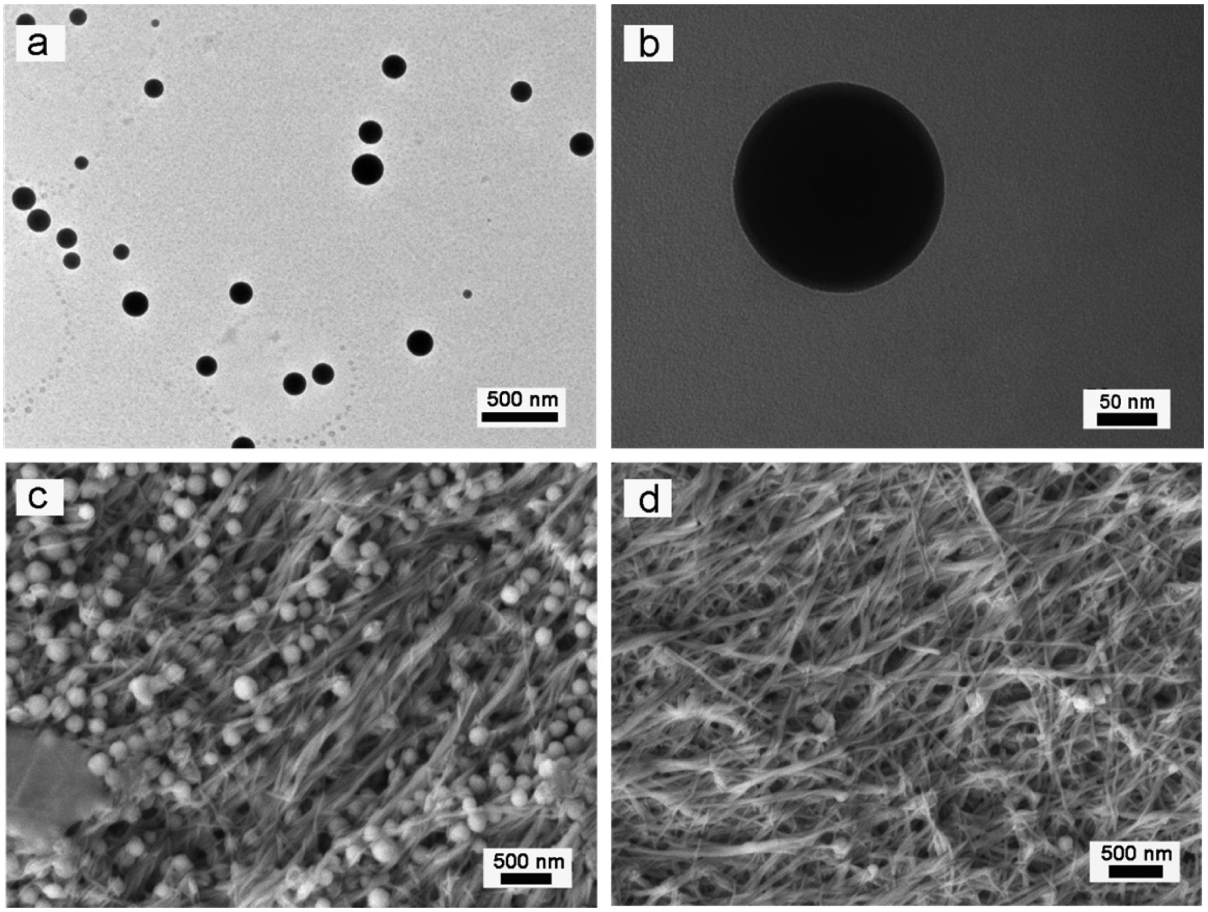

Figure 2. TEM images of the synthesized hybrid nanospheres with lower (a) and higher (b) magnification. SEM images of supramolecular structures formed by POM/[*N*-C_{10}, *N*′-COOH-Im]Br in the aqueous solution at room temperature after 4 (c) and 12 h (d), respectively.

Before each experiment, the glassy carbon electrode was polished with aluminum oxide, and modified with the as-prepared hybrid materials.

pH-Responsive Measurements. The pH of the hybrid solution was measured by a pH meter (PHS-3C, INESA). The initial pH was about 3.0, and then, the pH value of the solution was adjusted to 6.5 with diluted NaOH solution. Meanwhile, the macroscopic appearance of the solution underwent an obvious variation, namely, from turbid to transparent. The cycle experiments were carried out according to the above steps.

Adsorption Experiments. Aqueous solutions of POM/[*N*-C_{10}, *N*′-COOH-Im]Br (0.5 mM, 6.0 mL) and MO (1.2 mM, 2.0 mL) were added into a small tube (10 mL). The mixed solution was placed in a dark environment for a period of time. The 1 mL of the solution was used as the samples for UV−vis absorption measurements (HP 8453E in a quartz cell with 1 mm light path) after 0, 4, 8, 18, and 30 h, respectively.

Catalytic Experiments. The as-prepared POM/[*N*-C_{10}, *N*′-COOH-Im]Br hybrid solution (3.0 mL) and H_2O_2 (0.5 mL) solution were added to MO solution (1.2 mM, 2.0 mL) successively. The mixed solution was placed in an environment with or without sun light. The solution was monitored by UV−vis spectrometer after different times. The control experiments about MO degradation reaction in the presence of single POM or [*N*-C_{10}, *N*′-COOH-Im]Br or POM/[*N*-C_{10}, *N*′-Im]Br hybrid materials were also performed following the same experimental methods.

Characterizations of Supramolecular Structures. The chemical structures were ascertained by ^{1}H NMR (a Bruker Avance 300 spectrometer) and elemental analysis (Vario EL III elementar analyzer, Elementar) measurements. SEM images were recorded using a JEOL JSM-7600F at an accelerating voltage of 5 kV. TEM analysis was characterized in bright-field mode on a JEM-100X II(JEOL) electron microscope at an accelerating voltage of 120 kV. Small angle X-ray scattering (SAXS) measurements were performed using an Anton-paar SAX Sess mc^2 system with a Ni-filtered Cu Kα radiation (1.5406 Å) operated at 50 kV and 40 mA. Fourier transform IR (FTIR) spectra were determined by a VERTEX-70/70v FTIR spectrometer on pressed thin KBr disks of samples at room temperature. The diameter of particles was obtained by a laser particle analyzer (Delsa Nano_C, Beckmann, US) at 25 °C. The sample solutions were filtered through by 450 nm hydrophilic PVDF membrane filter (Millipore Durapore).

RESULTS AND DISCUSSION

Synthesis of the POM/SAIL Hybrid Materials. A single phase approach was adopted to prepare IL-encapsulated POM supramolecular complexes based on Keggin-type POM and [*N*-C_{10}, *N*′-COOH-Im]Br in the aqueous solution at room temperature. Monodispersed nanospheres with diameters of ca. 100−200 nm was clearly revealed by TEM images (Figure 2a, b) after the initial self-assembly process. These nanospheres then gradually transformed into nanofibril structures within 12 h (Figure 2d) and the intermediate state of the transformation could be shown in Figure 2c (4 h) and Figure S1, where both nanospheres and nanofibers existed. When the synthetic time of the materials was elongated to 24 h, all the nanospheres were observed to transform into nanofibers (Figure S2). These results indicate that the morphology of the obtained hybrid materials can be regulated by the synthetic time.

Characterizations of the POM/SAIL Hybrid Nanospheres. The composition of the hybrid materials was first investigated. ^{1}H NMR measurements were employed to confirm

DOI: 10.1021/acssuschemeng.6b02791
ACS Sustainable Chem. Eng. 2017, 5, 3650−3658

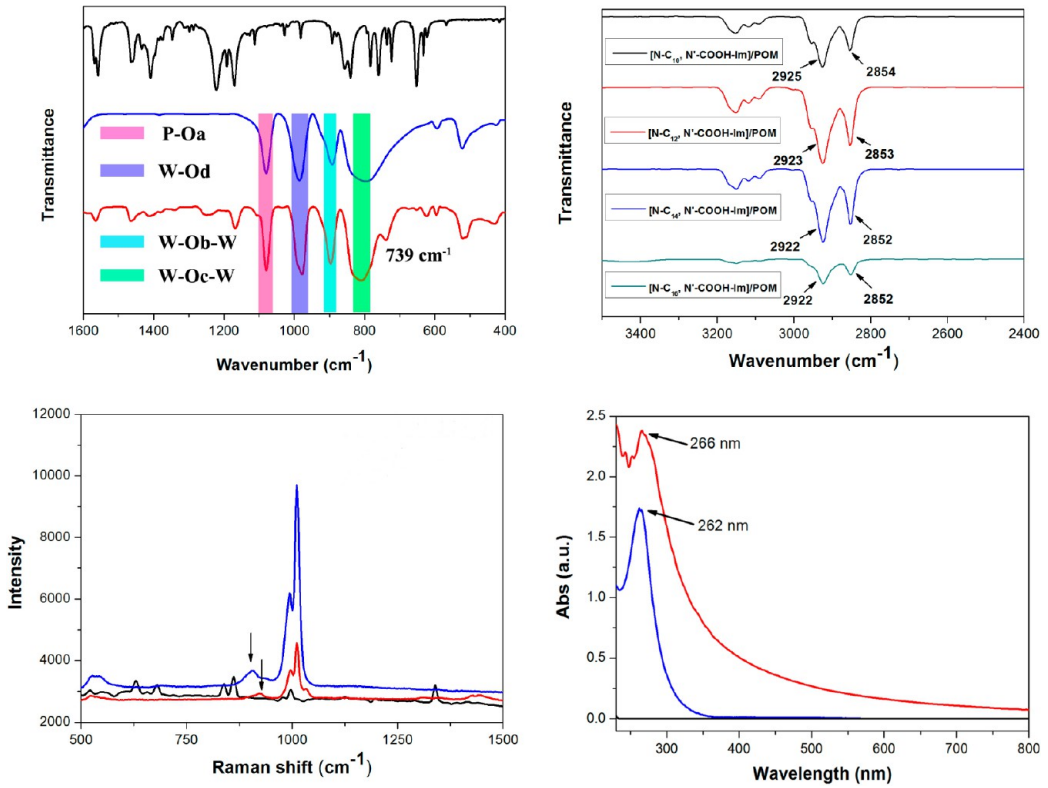

Figure 3. FTIR (a), Raman (c), and UV−vis (d) spectra of [*N*-C_{10}, *N*′-COOH-Im]Br (black curve), POM (blue curve), and POM/[*N*-C_{10}, *N*′-COOH-Im]Br hybrid materials (red curve). (b) FTIR patterns of POM/SAILs with different carbon chain length.

the formation of supramolecular materials and to investigate the interaction between POM and SAIL. Figure S3 shows the ^{1}H NMR spectra of [*N*-C_{10}, *N*′-COOH-Im]Br and the POM/[*N*-C_{10}, *N*′-COOH-Im]Br hybrid materials. It is found the proton peaks of [*N*-C_{10}, *N*′-COOH-Im]Br were well maintained in the ^{1}H NMR spectra of POM/[*N*-C_{10}, *N*′-COOH-Im]Br hybrid materials, which confirmed the existence of [*N*-C_{10}, *N*′-COOH-Im]Br in the supramolecular materials. Furthermore, the peak at 5.15 ppm assigned to the protons of $-CH_2-$ between the carboxyl group and the imidazolium cation shifts to 5.04 ppm, which illustrates the electrostatic interactions between cationic imidazolium group and anionic POM. Additionally, in consistence with the ^{1}H NMR, the FTIR characterization also suggests that the supramolecular materials are composed of [*N*-C_{10}, *N*′-COOH-Im]Br and POM. The FTIR spectrum of POM exhibits four characteristic vibration bands at 1079, 985, 892, and 796 cm^{-1}, respectively (Figure 3a). After complexation of POM with [*N*-C_{10}, *N*′-COOH-Im]Br, an obvious shift of the ν(W = O_d), ν(W−O_b−W) and ν(W−O_c−W) stretches were observed, indicating strong electrostatic interactions between POM and [*N*-C_{10}, *N*′-COOH-Im]Br.[31] The strong FTIR band at 1737 cm^{-1} for hybrid materials shifts about 8 cm^{-1} compared to pure [*N*-C_{10}, *N*′-COOH-Im]Br, which is attributed to C═O stretching vibrations. This peak shift may imply the existence of hydrogen bonding networks. In addition, a new band at 739 cm^{-1} branched from 809 cm^{-1} for W−Oc−W^{VI} is assigned to the hydrogen bond between [*N*-C_{10}, *N*′-COOH-Im]Br and O atom of W−Oc−W^{VI} (Figure 3a).[32] To further understand the self-assembly process of the POM hybrid materials, hydrophobic interaction of the alkyl chains of the SAILs was analyzed with the morphology and FTIR study. For the POM/[*N*-C_{10}, *N*′-COOH-Im]Br complex, the ν_{as} (CH_2) and ν_s (CH_2) FTIR bands appear at 2925 and 2854 cm^{-1}, respectively (Figure 3b), which indicates that *gauche* conformation existing in hybrid materials and alkyl chains are relatively disordered.[32] To confirm this effect is caused by the hydrophobic interaction of alkyl chains, we further changed the chain length of SAILs and synthesized [*N*-C_n, *N*′-COOH-Im]Br (n = 12, 14, 16). When [*N*-C_{12}, *N*′-COOH-Im]Br was used, the overall size of hybrid nanospheres obtained after 1 h became larger (300−500 nm; Figure 4a), in comparison with POM/[*N*-C_{10}, *N*′-COOH-Im] nanospheres. After 12 h, these [*N*-C_{12}, *N*′-COOH-Im]Br/POM hybrid materials could also transform into nanofibers in very high yield (Figure 4b). [*N*-C_{14}, *N*′-COOH-Im]Br and POM can also form hybrid nanospheres and fibers after 1 h (Figure 4c). However, when POM was added into the aqueous solution of [*N*-C_{16}, *N*′-COOH-Im]Br, the formed supramolecular complexes could not self-assemble into nanospheres and directly generated nanorods (Figure 4d). Indeed, the FTIR measurements upon these POM/SAIL hybrid materials may imply a similar trend. When the alkyl chain length of [*N*-C_n, *N*′-COOH-Im]Br increases from 10 to 12, 14, and 16; the FTIR spectra (Figure 3b) show that ν_{as} (CH_2) and ν_s (CH_2) bands of POM/[*N*-C_{10}, *N*′-COOH-Im]Br composites at 2925 and 2854 cm^{-1} shift to 2922−2923 and 2852−2853 cm^{-1}, respectively, which is more close to the high ordered alkyl chains at 2918 cm^{-1} (ν_{as} (CH_2)) and 2848 cm^{-1} (ν_s (CH_2)).[32] This illustrates the alkyl chains become more ordered with the increasing length of hydrophobic chain. Combining the morphological effect of the chain length, we believe the hydrophobic effect plays an important role in the formation of the highly monodisperse and uniform nanospheres.

Since Raman spectra are very sensitive to the differences in the external environment of POM, it can help to provide further

DOI: 10.1021/acssuschemeng.6b02791
ACS Sustainable Chem. Eng. 2017, 5, 3650−3658

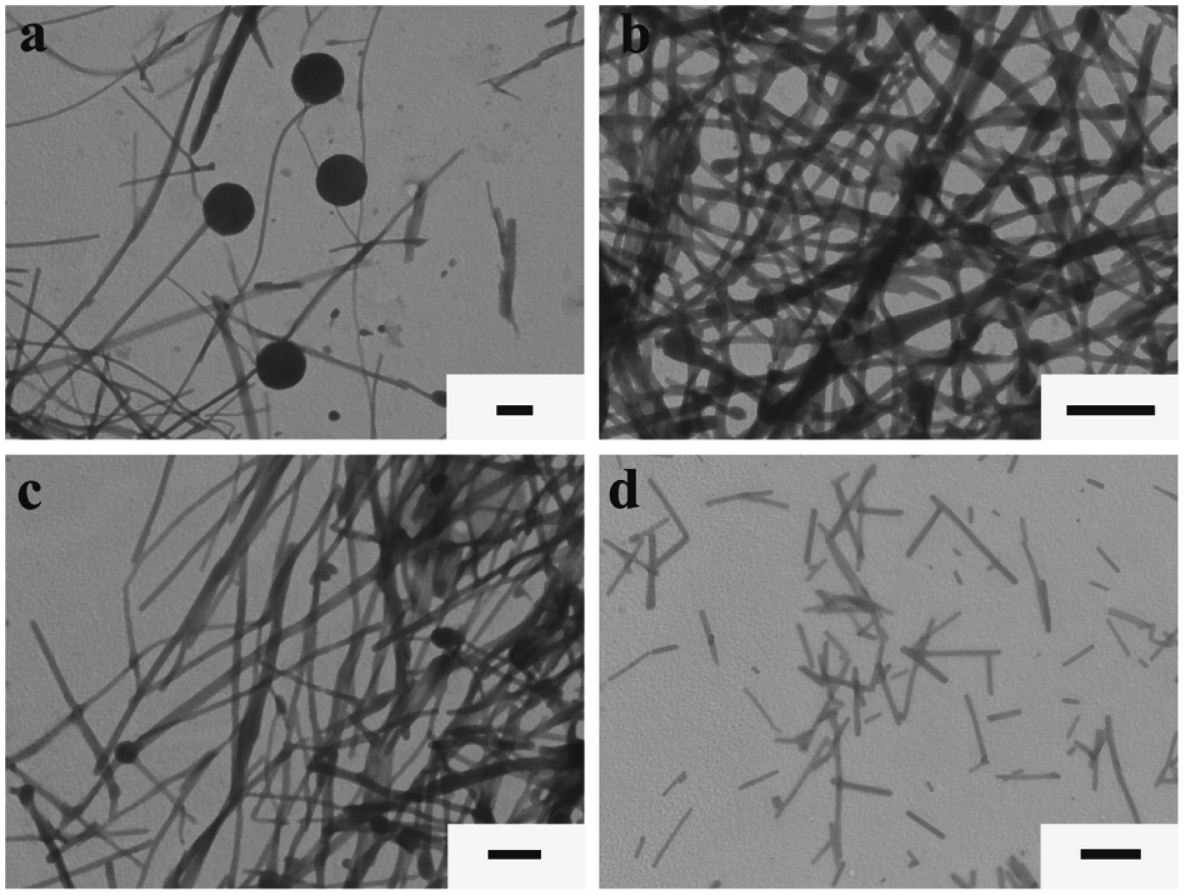

Figure 4. TEM images of supramolecular structures formed in the aqueous solution by POM/[*N*-C_{12}, *N*′-COOH-Im]Br after 1 h (a) and 12 h (b), POM/[*N*-C_{14}, *N*′-COOH-Im]Br (c), and POM/[*N*-C_{16}, *N*′-COOH-Im]Br (d) after 1 h at room temperature (the scale bar is 500 nm).

insight into hybrid materials. The Raman spectrum of POM exhibits three characteristic vibration bands at about 905, 993, and 1009 cm^{-1}, respectively (Figure 3c). Compared to pure POM, the band of [*N*-C_{10}, *N*′-COOH-Im]Br/POM hybrid materials around 920 cm^{-1} has a 15 cm^{-1} shift due to the electrostatic interactions.[33] UV−vis spectra (Figure 3d) show that the supramolecular materials have a strong characteristic absorption peak near 266 nm, which is ascribed to the O−W charge-transfer transition band.

Compared with the POM/[*N*-C_{10}, *N*′-COOH-Im]Br supramolecular complexes and pure POM, the UV−vis absorption is red-shifted by 4 nm, which can be attributed to dense arrangement and identical orientation of the hydrophobic chains of SAILs.[34] In SAXS diffractogram (Figure 5b), the ratio of the *q* values of the two scattering peaks is 1:2, suggesting the formation of highly ordered lamellar supramolecular structures. The calculated interplanar distance (d) of the typical lamellar structure is 3.1 nm. The energy minimized structures of [*N*-C_{10}, *N*′-COOH-Im]Br and POM molecules at the B3LYP/6-31G(d,p)[35] level are shown in Figure 5a, which demonstrates that the hydrophobic chain length of [*N*-C_{10}, *N*′-COOH-Im]Br is 1.36 nm and the width of POM is 0.52 nm (Figure 5a). Thus, the theoretical layer spacing (d_{theory}) is calculated as 1.88 nm. Apparently, the calculated interplanar distance (d) based on SAXS pattern is larger than the theoretical layer spacing (d_{theory}) but less than the twice of the value (3.76 nm).[36] Therefore, we determine the internal stacking of the POM/SAIL materials is in cross-bedding stacking mode, as shown in Figure 5c.

pH-Responsive Properties of the POM/SAIL Hybrid Nanospheres. As we demonstrated that the formation of the hybrid nanomaterials are based on the interaction between the SAIL and POM interface, the morphology of the POM/SAIL materials could in turn change accordingly to the environmental conditions. Herein, the concentration of H^+ ions (pH value) was able to induce the disassembly and assembly of the hybrid materials due to electrostatic repulsions between POM and the deprotonated SAIL. The difference in turbidity degree at different pH values was observed by dropwise adding 0.1 M NaOH aqueous solution to the dispersed POM/SAIL systems. Specifically, the hybrid nanospheres were in major when pH was about 3.0, leading to the high turbidity degree of the system, and the turbidity could reduce gradually with the increase of pH of the system. This process was reversible with the repeating change of pH values (Figure 6b), which was also confirmed in Figure 6a with DLS method. Such pH sensitivity may imply the significant role of electrostatic interactions in the formation and stability of the as-prepared nanospheres. When pH value changes from 3.0 to 6.5, −COOH of [*N*-C_{10}, *N*′-COOH-Im]Br becomes $-COO^-$. This transition could lead to stronger electrostatic repulsion between [*N*-C_{10}, *N*′-COO^--Im]Br molecules and POM clusters.

Catalytic Properties of POM-Based Hybrids: Degradation of Dyes. Since the POM materials are a family of widely used catalysts,[7,8] the POM/[*N*-C_{10}, *N*′-COOH-Im]Br supramolecular materials was also verified as a heterogeneous catalyst. The degradation of methyl orange (MO) in an aqueous solution was selected as a standard reaction to examine the catalytic

DOI: 10.1021/acssuschemeng.6b02791
ACS Sustainable Chem. Eng. 2017, 5, 3650−3658

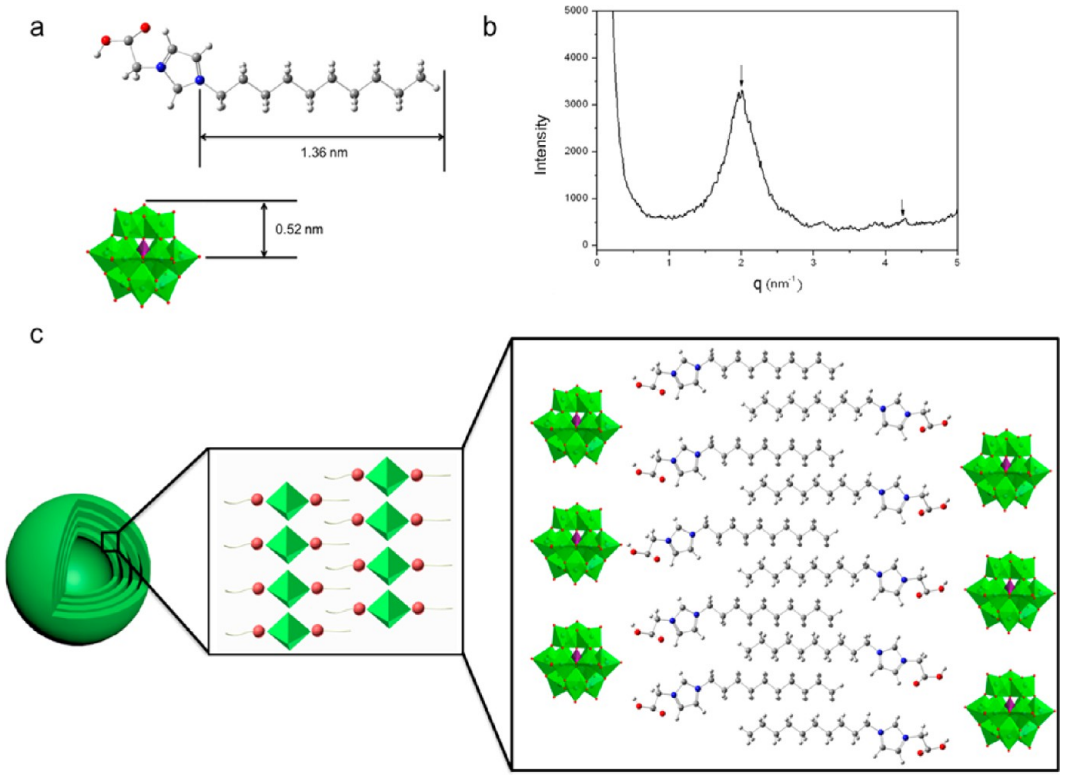

Figure 5. (a) Geometry of [*N*-C_{10}, *N*′-COOH-Im]Br optimized at the B3LYP/6-31G(d,p) level and schematic view of POM. (b) SAXS spectrum of POM/[*N*-C_{10}, *N*′-COOH-Im]Br hybrid materials. (c) Schematic illustration of the structure of POM/[*N*-C_{10}, *N*′-COOH-Im]Br hybrid materials.

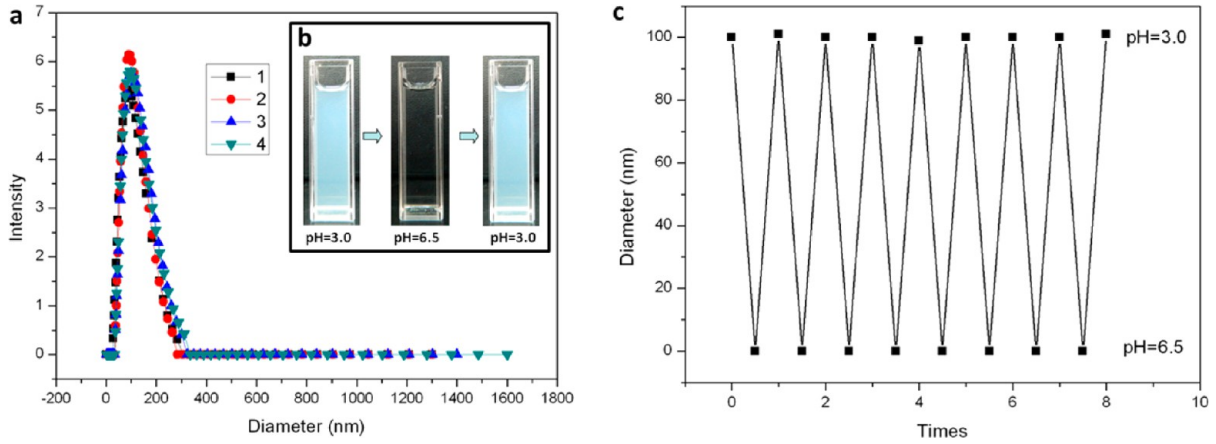

Figure 6. (a) DLS curves of the POM/[*N*-C_{10}, *N*′-COOH-Im]Br supramolecular nanospheres self-assembled at room temperature upon reversible changes of pH: curve 1 (black spots) initial state, curve 2 (red spots) encountering first cycle, curve 3 (blue spots) encountering second cycle, curve 4 (green spots) encountering third cycle. (b) Photographs showing reversible turbidimetric responses of the POM/[*N*-C_{10}, *N*′-COOH-Im]Br supramolecular nanospheres between pH 3.0 and 6.5 in water. (c) Mechanism for the pH-reversible turbidimetric responses of the POM/[*N*-C_{10}, *N*′-COOH-Im]Br supramolecular nanospheres.

efficiency of the POM-based hybrid materials. Based on previous reports, POM can activate H_2O_2 for the oxidation of organic compounds only under strong light irradiation (<400 nm), while in this work, highly efficient degradation of MO was achieved without light irradiation in the presence of H_2O_2 (Figure 7a, b, and curves 1 and 2 in c). In the control experiments, less degradation yields of MO were observed in POM/MO/H_2O_2 (curve 5 of Figure 7c) and [*N*-C_{10}, *N*′-COOH-Im]Br/MO/H_2O_2 (curve 6 of Figure 7c) systems. Such contrast sufficiently indicated the necessity of the hybrid materials containing the POM/SAIL interaction could catalyze the degradation in a high efficiency. In another control experiment, the absence of H_2O_2 greatly limited degradation of MO, indicating the catalytic role of POM/SAIL hybrid materials, rather than a reagent (Figure 7c, curve 3). Besides, to further prove the degradation reaction of MO, a control experiment containing POM/SAIL hybrid materials and MO was kept in dark without H_2O_2 added (curve 7 of Figure 7c). As a result, almost no change was observed for the concentration of MO with the elongation of time, implying that the decreases of MO concentration in other experiments (curve 1−6 in Figure 7c) were mainly caused by the degradation of MO molecules rather than the adsorption by the materials. The control experiments of MO/H_2O_2 in sunlight irradiation (curve 8 in Figure 7c) and

DOI: 10.1021/acssuschemeng.6b02791
ACS Sustainable Chem. Eng. 2017, 5, 3650−3658

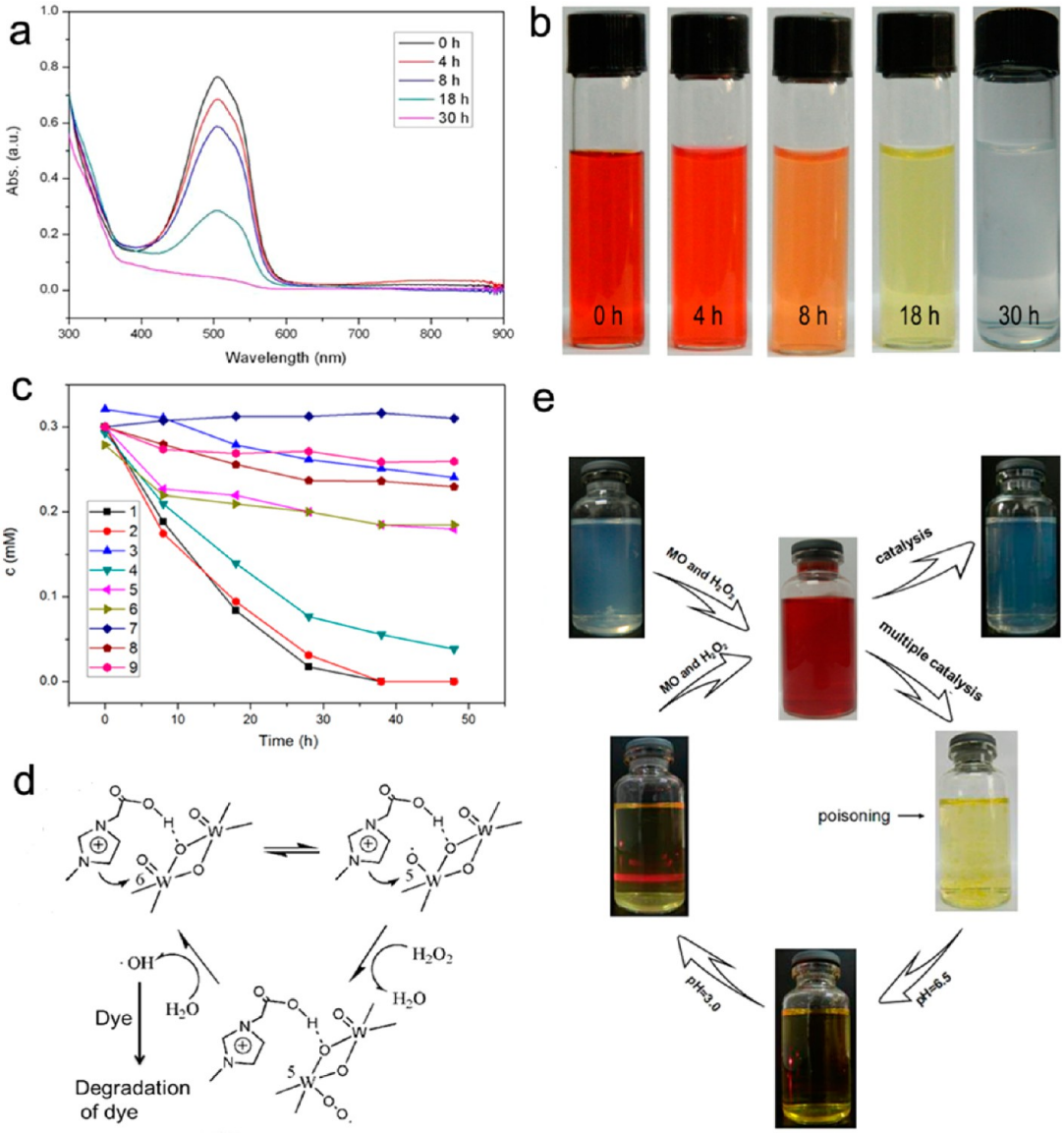

Figure 7. UV−vis spectra (a) and photographs (b) of degrading MO in the presence of the hybrid materials formed by POM/[*N*-C_{10}, *N*′-COOH-Im]Br and H_2O_2 at different time. (c) Plotted degradation kinetics of MO derived from UV−vis spectra (λ_{max} = 500 nm) in the hybrid materials/H_2O_2/MO system (sun light) (1), hybrid materials/H_2O_2/MO system (dark) (2), hybrid materials/MO system (sun light) (3), [*N*-C_{10}, *N*′-Im]Br/POM/H_2O_2/MO system (sun light) (4), POM/H_2O_2/MO system (sun light) (5), [*N*-C_{10}, *N*′-COOH-Im]Br/H_2O_2/MO system (sun light) (6), hybrid materials/MO system (dark) (7), H_2O_2/MO system (sun light) (8), and H_2O_2/MO system (dark) (9). (d) Proposed catalysis mechanism for heterogeneous degradation of MO catalyzed by POM/[*N*-C_{10}, *N*′-COOH-Im]Br hybrid materials in the presence of H_2O_2. (e) Schematic illustration of pH-induced recycle of POM/[*N*-C_{10}, *N*′-COOH-Im]Br materials.

in the dark (curve 9 in Figure 7c) show that only a little degradation of MO has occurred in either case. All the above results indicate that the degradation of MO is caused by the synergistic effect of the POM/SAIL hybrid materials and H_2O_2.

Based on the above results, the possible degradation mechanism of MO is proposed in Figure 7d. Based on the CV characterization, the hybrid materials inherited the good electrochemical properties of POM, which is the basis of the catalytic property (Figure S4). In a catalytic cycle, upon the contact of H_2O_2 on the surface of hybrid catalyst, an oxygen atom transfers from H_2O_2 to POM cluster to form the peroxide intermediate state, as indicated in the forward direction of Figure 7d. Subsequently, these highly active species attack and degrade the dye molecules, as indicated in the reverse direction of Figure 7d.[37] We also conducted a control experiment by using *N*-decyl-*N*′-methyl imidazolium bromide ([*N*-C_{10}, *N*′-Im]Br) to construct new hybrid materials with POM, which lacks a −COOH group, and therefore possesses a weaker interaction with POM. As a result, a remarkable decrease on the degradation efficiency was observed, implying H-bond between POM and SAIL molecules may impact on the catalytic activity of the hybrid materials (curve 4 of Figure 7c).

pH-Driven Regeneration of the Hybrid Catalyst. As a common issue, poisoning of catalyst widely exists in industrial production. After a catalyst is used for long time, it would adsorb residual organic molecules at the surfaces, resulting in the loss of the catalytic activity. Thus, the catalyst poisoning significantly shortens the lifetime of catalyst, causing a huge waste of resources. In our experiment, the hybrid catalyst material becomes yellow aggregates and loses activity after conducting the

DOI: 10.1021/acssuschemeng.6b02791
ACS Sustainable Chem. Eng. 2017, 5, 3650−3658

catalysis reaction for 6−8 times (Figure 7e). At this time, some residual organic molecules have already been absorbed on the catalyst surface and blocked the access to catalytic POM interface (Figure S5). As we have demonstrated, pH value of the aqueous solution can control disassembly and assembly of the hybrid nanospheres. Such method could also be used to address the poisoning problem of the catalyst. After poisoning of catalyst, when pH of the aqueous solution was adjusted to 6.5, the yellow aggregates in solution reduced gradually and the hybrid catalyst dissociated due to the electrostatic repulsions between POM and the deprotonated SAIL. However, the nanospheres could reform (Figure S6) after adjusting pH to 3.0, with the catalytic activity regenerated (Figure S7). So the catalyst poisoning issue is addressed by using the pH-responsive POM/[*N*-C_{10}, *N*′-COOH-Im]Br hybrid catalyst, which may avoid the common disadvantages of traditional catalysts. Our further investigation also confirmed that dyes, such as congo red and acid orange 7, could also be degraded using the POM/[*N*-C_{10}, *N*′-COOH-Im]Br hybrid catalyst with H_2O_2 as the oxidant. The simple and robust strategy reported in this study shows a promising prospect in regeneration of POM-based materials used for various catalytic reactions.

CONCLUSIONS

In summary, POM/[*N*-C_{10}, *N*′-COOH-Im]Br hybrid materials were first prepared in water via an ISA approach. Electrostatic interactions, hydrogen bonds, and hydrophobic interaction are the main driving forces for the formation of the hybrid materials that exhibit pH-responsive and renewable catalytic properties. Of particular interest is that disassembly and assembly of hybrid materials can be well-controlled by changing the pH of the aqueous solution, and this method was proven to be very promising to address the poisoning problem of catalyst. In addition, the catalytic reaction can also be conducted in dark. The smart supramolecular materials fabricated in this work are expected to solve poisoning of catalyst and reduce costs for industrial applications.

ASSOCIATED CONTENT

Supporting Information

The Supporting Information is available free of charge on the ACS Publications website at DOI: 10.1021/acssuschemeng.6b02791.

SEM image of POM/[*N*-C_{10}, *N*′-COOH-Im]Br standing for 4 h, TEM images POM/[*N*-C_{10}, *N*′-COOH-Im]Br standing for 24 h, and reformed nanospheres; ^{1}H NMR spectra of [*N*-C_{10}, *N*′-COOH-Im]Br, POM/[*N*-C_{10}, *N*′-COOH-Im]Br hybrid materials, and POM/[*N*-C_{10}, *N*′-COOH-Im]Br hybrid catalyst before and after poisoning; cyclic voltammograms of POM and POM/[*N*-C_{10}, *N*′-COOH-Im]Br hybrid materials, UV−vis spectra of MO after degradation for different time intervals using the regenerated hybrid catalyst (PDF)

AUTHOR INFORMATION

Corresponding Author

*E-mail: ylmlt@sdu.edu.cn.

ORCID

Li Yu: 0000-0002-7077-4760

Author Contributions

⊥Y.G. and Y.G. contributed to this work equally.

Notes

The authors declare no competing financial interest.

ACKNOWLEDGMENTS

This work was supported by the National Natural Science Foundation of China (No. 21373128), the Scientific and Technological Projects of Shandong Province of China (No. 2014GSF117001), the Natural Science Foundation of Shandong Province of China (No. ZR2011BM017), and the China Scholarship Council (CSC).

REFERENCES

(1) Stupp, S. I.; LeBonheur, V.; Walker, K.; Li, L. S.; Huggins, K. E.; Keser, M.; Amstutz, A. Supramolecular materials: self-organized nanostructures. *Science* **1997**, *276*, 384−389.

(2) De Greef, T. F.; Smulders, M. M.; Wolffs, M.; Schenning, A. P.; Sijbesma, R. P.; Meijer, E. Supramolecular polymerization. *Chem. Rev.* **2009**, *109*, 5687−5754.

(3) Finke, A. D.; Gross, D. E.; Han, A.; Moore, J. S. Engineering solid-state morphologies in carbazole-ethynylene macrocycles. *J. Am. Chem. Soc.* **2011**, *133*, 14063−14070.

(4) Zang, L.; Che, Y.; Moore, J. S. One-dimensional self-assembly of planar π-conjugated molecules: adaptable building blocks for organic nanodevices. *Acc. Chem. Res.* **2008**, *41*, 1596−1608.

(5) Milliron, D. J.; Buonsanti, R.; Llordes, A.; Helms, B. A. Constructing functional mesostructured materials from colloidal nanocrystal building blocks. *Acc. Chem. Res.* **2014**, *47*, 236−246.

(6) Dolbecq, A.; Dumas, E.; Mayer, C. R.; Mialane, P. Hybrid organic-inorganic polyoxometalate compounds: from structural diversity to applications. *Chem. Rev.* **2010**, *110*, 6009−6048.

(7) Kamata, K.; Yonehara, K.; Nakagawa, Y.; Uehara, K.; Mizuno, N. Efficient stereo- and regioselective hydroxylation of alkanes catalysed by a bulky polyoxometalate. *Nat. Chem.* **2010**, *2*, 478−483.

(8) Yang, Y.; Zhang, B.; Wang, Y.; Yue, L.; Li, W.; Wu, L. A Photo-driven Polyoxometalate Complex Shuttle and Its Homogeneous Catalysis and Heterogeneous Separation. *J. Am. Chem. Soc.* **2013**, *135*, 14500−14503.

(9) Tong, X.; Thangadurai, V. Hybrid Gel Electrolytes Derived from Keggin-Type Polyoxometalates and Imidazolium-Based Ionic Liquid with Enhanced Electrochemical Stability and Fast Ionic Conductivity. *J. Phys. Chem. C* **2015**, *119*, 7621−7630.

(10) Wu, Y.; Shi, R.; Wu, Y.-L.; Holcroft; Liu, J. M. Z.; Frasconi, M.; Wasielewski, M. R.; Li, H.; Stoddart, J. F. Complexation of Polyoxometalates with Cyclodextrins. *J. Am. Chem. Soc.* **2015**, *137*, 4111−4118.

(11) Li, H.; Qi, W.; Li, W.; Sun, H.; Bu, W.; Wu, L. A Highly Transparent and Luminescent Hybrid Based on the Copolymerization of Surfactant-Encapsulated Polyoxometalate and Methyl Methacrylate. *Adv. Mater.* **2005**, *17*, 2688−2692.

(12) Zhang, H.; Lin, X.; Yan, Y.; Wu, L. Luminescent logic function of a surfactant-encapsulated polyoxometalate complex. *Chem. Commun.* **2006**, 4575−4577.

(13) Wang, J.; Han, D.; Wang, X.; Qi, B.; Zhao, M. Polyoxometalates as peroxidase mimetics and their applications in H_2O_2 and glucose detection. *Biosens. Bioelectron.* **2012**, *36*, 18−21.

(14) Mercier, D.; Ben Haddada, M.; Huebner, M.; Knopp, M. D.; Niessner, R.; Salmain; Proust, M.; Boujday, A. S. Polyoxometalate nanostructured gold surfaces for sensitive biosensing of benzo[a]-pyrene. *Sens. Actuators, B* **2015**, *209*, 770−774.

(15) Zhang, Y.; Bo, X.; Nsabimana, A.; Munyentwali, A.; Li, M.; Guo, L.; Han, C. Green and facile synthesis of an Au nanoparticles@ polyoxometalate/ordered mesoporous carbon tri-component nanocomposite and its electrochemical applications. *Biosens. Bioelectron.* **2015**, *66*, 191−197.

(16) Fu, L.; Gao, H.; Yan, M.; Li, S.; Li, X.; Dai, Z.; Liu, S. Polyoxometalate-Based Organic-Inorganic Hybrids as Antitumor Drugs. *Small* **2015**, *11*, 2938−2945.

DOI: 10.1021/acssuschemeng.6b02791
ACS Sustainable Chem. Eng. 2017, 5, 3650−3658

(17) Geisberger, G. E.; Gyenge, B.; Hinger, D.; Bösiger, P.; Maake, C.; Patzke, G. R. Synthesis, characterization and bioimaging of fluorescent labeled polyoxometalates. *Dalton Trans.* **2013**, *42*, 9914−9920.
(18) Gong, Y.; Hu, Q.; Cheng, N.; Wang, T.; Xu, W.; Bi, Y.; Yu, L. Fabrication of pH- and temperature-directed supramolecular materials from 1D fibers to exclusively 2D planar structures using an ionic self-assembly approach. *J. Mater. Chem. C* **2015**, *3*, 3273−3279.
(19) Landsmann, S.; Luka, M.; Polarz, S. Bolaform surfactants with polyoxometalate head groups and their assembly into ultra-small monolayer membrane vesicles. *Nat. Commun.* **2012**, *3*, 1299−1034.
(20) Li, H.; Sun, H.; Qi, W.; Xu, M.; Wu, L. Onionlike Hybrid Assemblies Based on Surfactant-Encapsulated Polyoxometalates. *Angew. Chem., Int. Ed.* **2007**, *46*, 1300−1303.
(21) Nisar, A.; Lu, Y.; Zhuang, J.; Wang, X. Polyoxometalate Nanocone Nanoreactors: Magnetic Manipulation and Enhanced Catalytic Performance. *Angew. Chem., Int. Ed.* **2011**, *50*, 3187−3192.
(22) Yan, Y.; Wang, H.; Li, B.; Hou, G.; Yin, Z.; Wu, L.; Yam, V. W. W. Smart Self-Assemblies Based on a Surfactant-Encapsulated Photoresponsive Polyoxometalate Complex. *Angew. Chem., Int. Ed.* **2010**, *49*, 9233−9236.
(23) Li, W.; Yin, S.; Wang, J.; Wu, L. Tuning mesophase of ammonium amphiphile-encapsulated polyoxometalate complexes through changing component structure. *Chem. Mater.* **2008**, *20*, 514−522.
(24) Leng, Y.; Wang, J.; Zhu, D.; Zhang, M.; Zhao, P.; Long, Z.; Huang, J. Polyoxometalate-based amino-functionalized ionic solid catalysts lead to highly efficient heterogeneous epoxidation of alkenes with H2O2. *Green Chem.* **2011**, *13*, 1636−1639.
(25) Biboum, R. N.; Doungmene, F.; Keita, B.; de Oliveira, P. D.; Nadjo, L.; Lepoittevin, B.; Roger, P.; Brisset, F.; Mialane, P.; et al. Poly(ionic liquid) and macrocyclic polyoxometalate ionic self-assemblies: new water-insoluble and visible light photosensitive catalysts. *J. Mater. Chem.* **2012**, *22*, 319−323.
(26) Faul, C. F.; Antonietti, M. Ionic self−assembly: Facile synthesis of supramolecular materials. *Adv. Mater.* **2003**, *15*, 673−683.
(27) Dolbecq, A.; Mialane, P.; Keita, B.; Nadjo, L. Polyoxometalate-based materials for efficient solar and visible light harvesting: application to the photocatalytic degradation of azo dyes. *J. Mater. Chem.* **2012**, *22*, 24509−24521.
(28) Gkika, E.; Troupis, A.; Hiskia, A.; Papaconstantinou, E. *Appl. Catal., B* **2006**, *62*, 28−34.
(29) Kim, S.; Yeo, J.; Choi, W. Photocatalytic reduction of chromium and oxidation of organics by polyoxometalates. Simultaneous conversion of dye and hexavalent chromium in visible light-illuminated aqueous solution of polyoxometalate as an electron transfer catalyst. *Appl. Catal., B* **2008**, *84*, 148−155.
(30) Rezaeifard, A.; Haddad, R.; Jafarpour, M.; Hakimi, M. Catalytic Epoxidation Activity of Keplerate Polyoxomolybdate Nanoball toward Aqueous Suspension of Olefins under Mild Aerobic Conditions. *J. Am. Chem. Soc.* **2013**, *135*, 10036−10039.
(31) Yan, X.; Zhu, P.; Fei, J.; Li, J. Self-Assembly of Peptide-Inorganic Hybrid Spheres for Adaptive Encapsulation of Guests. *Adv. Mater.* **2010**, *22*, 1283−1287.
(32) Zhang, T.; Spitz, C.; Antonietti, M.; Faul, C. F. J. Highly Photoluminescent Polyoxometaloeuropate-Surfactant Complexes by Ionic Self-Assembly. *Chem. - Eur. J.* **2005**, *11*, 1001−1009.
(33) Rao, K. N.; Dingwall, L. D.; Gai, P. L.; Lee, A. F.; Tavener, S. J.; Young, N. A.; Wilson, K. Synthesis and characterization of nanoporous phospho-tungstate organic-inorganic hybrid materials. *J. Mater. Chem.* **2008**, *18*, 868−874.
(34) Zhang, T. R.; Feng, W.; Fu, Y. Q.; Lu, R. C.; Bao, Y. X.; Zhang, T.; Zhao, B.; Sun, C. Q. T.; Li, J.; Zhao, Y. Y.; Yao, J. N. Self-assembled organic−inorganic composite superlattice thin films incorporating photo- and electro-chemically active phosphomolybdate anion. *J. Mater. Chem.* **2002**, *12*, 1453−1458.
(35) Frisch, M. J.; Trucks, G. W.; Schlegel, H. B.; Scuseria, G. E.; Robb, M. A.; Cheeseman, J. R.; Scalmani, G.; Barone, V.; Mennucci, B.; Petersson, G. A.; Nakatsuji, H.; Caricato, M.; Li, X.; Hratchian, H. P. A. F.; Bloino, J.; Zheng, G. J.; Sonnenberg, L.; Hada, M.; Ehara, M.; Toyota, K.; Fukuda, R.; Hasegawa, J.; Ishida, M.; Nakajima, T.; Honda, Y.; Kitao, O.; Nakai, H.; Vreven, T.; Montgomery, J. A.; Peralta, J. J. E.; Ogliaro, F.; Bearpark, M.; Heyd, J. J.; Brothers, E.; Kudin, K.; Staroverov, N. V. N.; Kobayashi, R.; Normand, J.; Raghavachari, K.; Rendell, A. J.; Iyengar, C.; Tomasi, S. S.; Cossi, J.; Rega, M.; Burant, N. J.; Millam, M.; Klene, M.; Knox, J. E.; Cross, J. B.; Bakken, V.; Adamo, C.; Jaramillo, J.; Gomperts, R.; Stratmann, R. E.; Yazyev, O. A.; Austin, J.; Cammi, R.; Pomelli, C. J.; Ochterski, W.; Martin, R. L.; Morokuma, K. V.; Zakrzewski, G.; Voth, G. A.; Salvador, P.; Dannenberg, J. J.; Dapprich, S.; Daniels, A. D.; Farkas, O.; Foresman, J. B.; Ortiz, J. V.; Cioslowski, J.; Fox, D. J. R. A. *Gaussian 09*; Gaussian Inc., Wallingford CT, 2009.
(36) Ramakanth, I.; Ramesh, N.; Patnaik, A. Fibrous gels of cetylpyridinium chloride in binary solvent mixtures: structural characteristics and phase behavior. *J. Mater. Chem.* **2012**, *22*, 17842−17847.
(37) Chen, C.; Wang, Q.; Lei, P.; Song, W.; Ma, W.; Zhao, J. Photodegradation of dye pollutants catalyzed by porous $K_3PW_{12}O_{40}$ under visible irradiation. *Environ. Sci. Technol.* **2006**, *40*, 3965−3970.

DOI: 10.1021/acssuschemeng.6b02791
ACS Sustainable Chem. Eng. 2017, 5, 3650−3658